Mobile and self-powered battery energy storage system in distribution networks–Modeling, operation optimization, and comparison with stationary counterpart

Hedayat Saboori , Shahram Jadid [*]

Center of Excellence for Power System Automation and Operation, Electrical Engineering Department, Iran University of Science and Technology, Tehran, Iran

ARTICLE INFO

ABSTRACT

Spatio-temporal and power-energy controllability of the mobile battery energy storage system (MBESS) can offer various benefits, especially in distribution networks, if modeled and employed optimally. Accordingly, this paper presents a novel and efficient model for MBESS modeling and operation optimization in distribution networks. Given the transportation sector's transition towards electrification, a self-powered electric truck is considered for conveying the whole battery system. As a result, the required energy for transportation is obtained from the main battery system. The proposed model demands only transportation time between distribution network buses without modelling the whole transportation network. Novel straightforward and efficient formulations consider transportation time and cost limitations by linear equations capable of handling real-world systems without dimensionality problems. The model is implemented on a sample system, and its results are compared with the stationary batteries. The simulation results demonstrate the proposed model's effectiveness to obtain a minimum cost operation plan accompanied by the enhanced technical performance compared to the stationary battery installations. By employing the MBESS in a typical distribution network, the total operation cost is reduced by more than 4%, while total losses and maximum substation power are reduced by, in turn, 740 kWh and 690 kVA.

1. Introduction

Implementing modern smart grids necessitates deploying energy storage systems. These systems are capable of storing energy for delivery at a later time when needed [1]. Depending on the type and application, the period between the charging and discharging of these devices may vary from a few seconds to even some months [2,3]. Shorter time periods of storage, which may range from a few seconds to a few minutes, can be attributed to fast storage systems such as supercapacitors, superconducting magnetic energy storage (SMES), flywheel energy storage, and high energy density batteries. They are mainly used in power quality applications or smoothing short-term variations of renewable resources [4,5]. More extended periods of energy storage are often provided by high-density batteries, pumped hydro energy storage, compressed air energy storage (CAES), or hydrogen storage. These

storages, capable of transmitting energy from hours to even months, are suitable for energy management applications such as arbitrage, pick shaving, expansion deferral, or the time-shift of renewable sources [6].

Among the above storage devices, only battery technologies can provide both types of applications [7]. Accordingly, batteries have been the pioneering technology of energy storage, and many studies have been done over the past decade on their types, applications, features, operation optimization, and scheduling, especially in distribution networks [8]. Along with research studies, many power companies worldwide have installed or plan to increase the installed capacity of utility-scale batteries [9]. The battery systems have the potential of mobility in the grid due to their high energy and power density and modular structure. Besides, the ability to connect quickly and easily, the silent operation, and no need for particular installation and construction conditions make it easy to move within the network [10]. In this case,

---

* Corresponding author.
  E-mail addresses: h_saboori@elec.iust.ac.ir (H. Saboori), jadid@iust.ac.ir (S. Jadid).

the MBESS can charge and discharge in different locations depending on the situation. Accordingly, the battery will also be able to shift the stored energy, both spatially and temporally. This spatio-temporal energy transport will increase the benefits of the MBESS compared to its stationary counterpart. The idea of using the MBESS was first introduced by the Electric Power Research Institute (EPRI) in 2008 [11]. The institute tackled the topic in a research project called the ``Transportable Energy Storage System Project''. As stated in the objectives of this project, transportable storage devices can be used to manage load growth and assist in the operation of distribution networks. The focus of the project was on the possibility of transporting different types of batteries. The authors in [12] have presented a model based on a metaheuristic method (particle swarm optimization) for MBESS energy management in distribution networks. The primary purpose of the MBESS utilization was to reduce the transmitted energy from the upstream network by maximizing the use of renewable resources in the distribution network.

Managing the high shares of renewable energies in electric power distribution networks has always been a challenge due to their intermittence nature. One of the methods to tackle this problem is to use storage devices. The authors in [13] have been proposed to use mobile batteries for this purpose. Accordingly, a multi-stage mobile batteries transportation and logistics scheduling method was proposed. The proposed method aimed at enhancing renewable energy hosting capacity and system economics. In this way, the mobile batteries will be charged at renewable energy power stations and moved backed to the load centers by railways. In the study conducted in [14], a two-stage mathematical programming method was presented that simultaneously optimized mobile batteries' investment and operation in distribution networks. The mobile battery was used to form dynamic microgrids in severe disasters and enhance system resilience. Similarly, the authors in [15] aimed to increase the distribution network's resilience through mobile resources management. A mobile battery system can offer multiple stacked services similar to a stationary installation. This capability was focused on in [16], wherein a sizing method is proposed for mobile batteries. The allocation criterion was based on achieving multiple services, including load leveling, peak shaving, voltage profile improvement, and renewable energy integration. Also, load and renewable energy fluctuations, in addition to the market price changes, were considered. Afterward, in [17], a remote microgrid formation method was proposed based on MBESS deployment. Finally, in [18] and [19], the reliability evaluation of mobile storage systems was researched. An MBESS may be compared with a coordinated scheduling scheme of an Electric Vehicle (EV) fleet. The merits and demerits of using coordinated EVs to achieve an aggregate storage capacity are previously assessed in the literature [20]. The advantages of the MBESS over an EV fleet can be compared as follows.

1. Owners' unwillingness to be controlled: typically, the EV owners are unwilling to be controlled and scheduled by a central agent. This type of control reminds car owners that they do not own the car coordinated and have borrowed the car somehow. This makes social acceptance of the coordinated control of electric vehicles for network purposes a critical issue. There is no such problem with the MBESS.
2. Unclear payment and participation mechanism: there is no clear participation and payment mechanism for coordinated EV scheduling. Even if car owners are willing to participate in the scheme, there should be a precise mechanism for participating and being paid. This mechanism should consider the amount of power and energy purchased from the car and the time and place of use. The practical design and implementation of such a mechanism are critical challenges given the wide range of vehicles and their owners' attitudes.
3. Unawareness of EVs' state of charge: Accurately estimating the total energy available from the vehicles is a very complex task. Due to the EV battery degradation over time and the variable number and scheme of participation of cars in the program, the total amount of power and energy available cannot be readily determined.
4. Model complexity and tractability: Even if the above problems are targeted using advanced mathematical models, the resulting formulation will be very large-scale and with a substantial computational burden. This will cause severe problems in convergence and runtime, especially in real distribution networks with a very high number of buses. For each vehicle, at least some specific binary and continuous variables must be considered to determine the temporal-spatial status, participation mechanism in the program, and power and energy for each hour of schedule. As a result, the dimensions of the problem will increase exponentially as the number of vehicles increases.
5. Battery degradation and related costs for the EVs owners: Using EVs batteries for energy and power management applications in the network will significantly reduce their lifespan. The battery health is a function of the number of charge and discharge times as well as the discharge depth. Determining the exact amount of battery life reduction and induced cost resulting from utilization by the network operator is very complicated. Given that the EV battery is also depreciated due to daily use by the owner, it is complicated to determine the share of each factor.

It should be noted that the primary requirement for deploying a mobile battery is precise modeling of its spatio-temporal behavior and optimization of the operation based on the obtained model. In previous studies, high-dimensional variables have been used for modeling, or the number of constraints was relatively high due to transportation network modeling. Besides, the self-supplying mechanism for the truck conveying the battery system is not included. Given the transportation industry's transition towards electric vehicles and the fact that the battery carries electrical energy, this feature must be considered. Also, no comparison study has been performed between mobile and stationary batteries under normal network operation. In this paper, the research gaps mentioned above are targeted by presenting a new mathematical model. The proposed model does not require modeling the traffic network and only requires the transportation time between network buses. The truck-mounted by the battery system container is electric and receives the energy needed for movement from the battery itself. Straightforward relations consider the transportation time limit required to move between the network buses. A cost term is also considered for the daily cost of battery operation, typically the driver's cost without adding the new variables. The final mathematical model is Mixed Integer Linear Programming (MILP). As a result, it can integrate into the commercial distribution network operation and optimization software packages used for very large-scale real-life systems without divergence problems and guaranteed convergence to the global optima. The model is implemented on a sample system, and its results are compared and analyzed with a stationary battery installed in the network buses. In summary, the innovations of this paper can be listed as follows.

- Efficient modelling of MBESS transportation time and cost with low computational burden.
- Modelling self-powering mechanism for the electric truck conveying the whole battery system.
- Linear model capable of handling real-world systems without dimensionality concerns.
- Requiring only transportation time between network buses

The rest of the paper is ordered as follows. In Section 2, the proposed spatio-temporal mobile battery model is introduced. In this section, the physical concept of battery movement is first described, and then the mathematical model is extracted. Next, in Section 3, the proposed model is integrated into the distribution network's optimal daily operation schedule. Then, a case study is implemented to evaluate the

functionality of the proposed model in Section 4. Finally, Section 5 presents the concluding remarks of the research.

2. Spatio-temporal operation model of MBESS

Fig. 1 depicts the general rules of mobile battery operation in the distribution network. The whole battery system comprising storage cells, a bidirectional power converter, and the transformer (if needed) is compacted and placed in a container. The whole battery system container is mounted on a truck to be movable [21]. The truck-mounted battery system, or equivalently Mobile Battery Energy Storage System (MBESS), can move across the network for charging and discharging if connected to a bus. The black-filled circles denote distribution network buses (denoted by sets i and j). The MBESS may be connected to one of the network buses or on the road at any time period of operation (indexed by sets t and u). Connection of the MBESS to the network buses is essential for charging or discharging. Before starting the mathematical modeling of the MBESS operation, its spatio-temporal status has to be defined. In other words, the MBESS spatial status at any time period of operation must be determined. Accordingly, the binary variable $Z_{(i,t)}^{MB}$ is used to denote spatio-temporal status of the MBESS. This variable indicates the connection of the MBESS to bus i at time period t, if switched on. Otherwise, the zero value of spatio-temporal variable indicates the transportation of the MBESS. This two-dimensional binary variable is used to model various operation constraints of the MBESS in the following.

As shown in Fig. 1, the MBESS can connect to at most one of the network buses at any time period. This limitation is mathematically modeled by (1). Besides, the MBESS starts daily operation horizon with a predefined spatio-temporal status. It has to be relocated to this status at the end of the time periods (T), as denoted by (2).

$$\sum_i Z_{(i,t)}^{MB} \leq 1 \quad \forall\, t \tag{1}$$

$$Z_{(i,t)}^{MB} = Z_{Ini}^{MB} \quad \forall\, i, t = T \tag{2}$$

Moving the MBESS between different bus locations necessitate spending a specific time on the road. This time, movement time between buses is the only input required for MBESS modeling related to the traffic medium. A matrix is used to denote these time values considering bidirectional nature, shown by *TM* in (3).

$$TM = \begin{bmatrix} TM_{1,1} & TM_{1,2} & TM_{1,3} & \dots & TM_{1,J} \\ TM_{2,1} & \ddots & & & \vdots \\ TM_{3,1} & & \ddots & & \vdots \\ \dots & & & \ddots & \vdots \\ TM_{I,1} & \dots & \dots & \dots & TM_{I,J} \end{bmatrix} \quad \forall\, i,j \in A_I \tag{3}$$

It should be noted that the *Tm* values are only movement time and not the total time required for changing the MBESS connection bus location. In other words, changing the MBESS connection locations necessitates detaching the previous bus connection, the movement to the new location, and then attaching it to the new bus. Accordingly, the constant times required for disconnection and connection of the MBESS to the network buses must add to the $TM_{(i,j)}$ to constitute the Total Transportation Time for each movement ($TT_{(i,j)}$), as shown in (4). In this equation, *TC* and *TD* are constant connection and disconnection time.

$$TT_{(i,j)} = TD + TM_{(i,j)} + TC \quad \forall\, i,j \in A_I \tag{4}$$

The $TT_{(i,j)}$ has to be regarded when the MBESS changes its bus location over time. In other words, the MBESS is allowed to connect to the location if the corresponding total transportation time regarding the destination bus location is elapsed. This limitation is modelled in (5) and (6). Based on (5), the battery can travel from bus i at time *t* to bus *j* at time u, if the time interval between *t* and *u* is as long as the total time required to transport between buses *i* and *j*, namely $TT_{(i,j)}$. Another point to note is that after passing the required transport time, the battery must be connected. In other words, the non-connection time of the battery cannot be longer than the required total transport time, which is considered by adding (6).

$$Z_{(i,t)}^{MB} + Z_{(j,u)}^{MB} \leq 1 \quad \forall\, t \in A_T,\, \{i,j\} \in A_I,\, i \neq j,\, u = \{t+1, ..., t + TT_{(i,j)}\} \tag{5}$$

$$\sum_{u=t+1}^{t+TT_{(i,j)}+1} \left[Z_{(j,u)}^{MB} \right] \geq Z_{(i,t)}^{MB} \quad \forall\, t \in A_T,\, \{i,j\} \in A_I \tag{6}$$

In addition to transportation time, the truck driver's driving cost must be considered in the MBESS operation. A constant daily driver cost
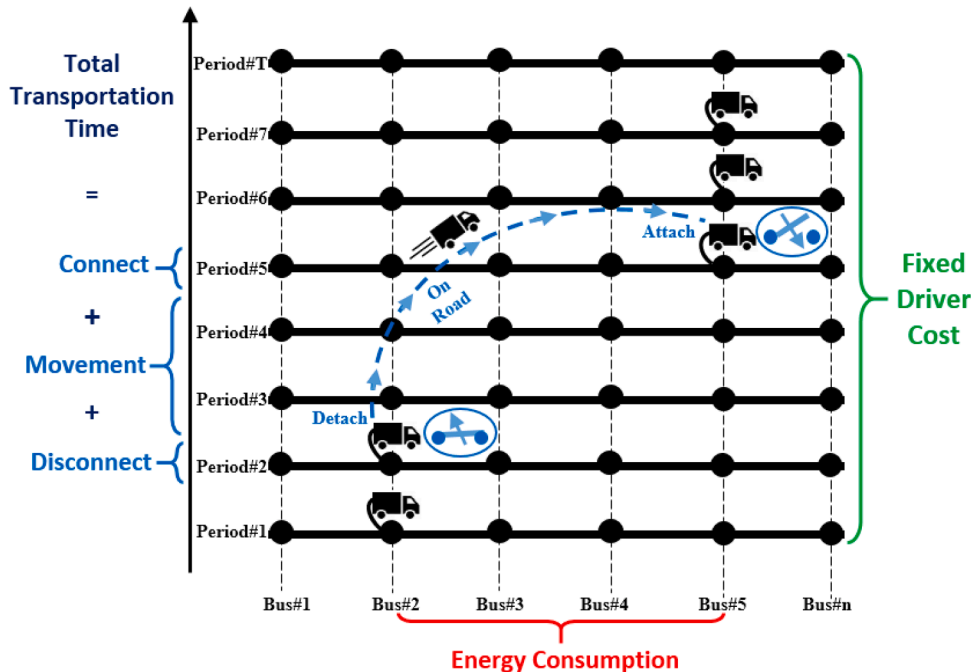
Fig. 1. General rules of MBESS operation.

is considered regardless of the MBESS operation pattern. This consideration is compatible with real-world situations when hiring a set of driver human resources. It should be noted that the driver(s) is (are) educated and responsible for the connection and disconnection of the MBESS to the network besides driving the truck. The constant driver cost, C_{Dr}^{MB}, is added to the other cost terms to form the total daily operation cost in the following. As mentioned previously, the truck conveying the battery container is electric and self-powered. The energy required for the truck movement is calculated in (7). The equation presents an hourly energy consumption term, $J_{(t)}^{TR}$, denoting truck movement. Hourly transportation of the truck is determined by detecting zero values of the binary spatio-temporal variable over all network buses. in other words, If the value of the variable is zero for all buses at a certain period of time, it means that the truck is not connected and is therefore on the road. The required energy for movement is then easily calculated by multiplying hourly unit energy required (F_E^{TR}) in an hour movement. This energy term is then subtracted from the stored energy in the battery.

$$J_{(t)}^{TR} = F_E^{TR} \sum_i \left(1 - Z_{(i,t)}^{MB}\right) \quad \forall t \in A_T \tag{7}$$

Fig. 2 demonstrates various parts of the MBESS inside the truck-mounted container. As in the figure, the primary part of the system is the storage cells pack. The storage cells receive, store, and inject DC power. A bidirectional power converted is used to connect the cells to the AC utility distribution grid. The power converter may work either at the rectifier (charging mode) or inverter (discharging mode). The reactive power is produced (or consumed) and controlled in this stage by the power converter. The commercial utility-scale battery system can absorb and inject active and reactive power in a fully four-quadrant manner. This capability is modeled in the following. If the battery must be connected to the medium voltage distribution network, a transformer is also used.

Fig. 3 demonstrates the relation between the active and reactive powers of the battery. There are some technical rules and limitations which have to be observed. The active and reactive power of the battery is independent of each other in any direction. However, the battery can only be charged or discharged at any time period. The charging and discharging modes used for active power are equivalent to inductive and capacitive modes for reactive power. Besides, the battery can interact with active and reactive power with the grid if connected to one of the buses. As shown in the figure, the active power interlock enforces the battery to choose only one of the charging or discharging active powers if the battery is connected to the network. Similarly, the reactive power interlock allows the battery to select inductive or capacitive reactive power if connected to the network. Additionally, the battery's output power is a mixture of active and reactive power, namely apparent power. Finally, each of the active, reactive, or apparent power in any direction must be less than the rated power of the MBESS.

The active power interlock between charging and discharging modes is simulated using two indicator binary variables. The charging ($X_{(i,t)}^{BC}$)

and discharging ($X_{(i,t)}^{BD}$) binary variables in (8) allow the battery to pass the active power if the corresponding spatio-temporal binary variable is switched-on previously. Based on (9), the battery can receive active power to be charged $P_{(i,t)}^{BC}$ as large as its rated power (S^{MB}) if the corresponding charging variable is switched-on. A similar situation is established in (10) when the battery is discharged by $P_{(i,t)}^{BD}$ [22].

$$X_{(i,t)}^{BC} + X_{(i,t)}^{BD} \leq Z_{(i,t)}^{MB} \quad \forall i, t \tag{8}$$

$$P_{(i,t)}^{BC} \leq X_{(i,t)}^{BC} S^{MB} \quad \forall i, t \tag{9}$$

$$P_{(i,t)}^{BD} \leq X_{(i,t)}^{BD} S^{MB} \quad \forall i, t \tag{10}$$

The limitations modeled above for active powers are simulated for reactive power in (11)–(13). In this relations, $Y_{(i,t)}^{BI}$ and $Y_{(i,t)}^{BC}$ represents indicator binary variables for inductive and capacitive reactive flow while $Q_{(i,t)}^{BI}$, and $Q_{(i,t)}^{BC}$ stand for corresponding reactive powers [23].

$$Y_{(i,t)}^{BI} + Y_{(i,t)}^{BC} \leq Z_{(i,t)}^{MB} \quad \forall i, t \tag{11}$$

$$Q_{(i,t)}^{BI} \leq Y_{(i,t)}^{BI} S^{MB} \quad \forall i, t \tag{12}$$

$$Q_{(i,t)}^{BC} \leq Y_{(i,t)}^{BC} S^{MB} \quad \forall i, t \tag{13}$$

Vector summation over active and reactive power of the battery is equal to the apparent power flowing through it. This value should be lower than the battery's rated power, as established in (14). To avoid non-linearity, this constraint is rewriting as (15) by using (16) and (17). In this method, the original binding circle is approximated by a set of m lines (linear equations), as shown in Fig. 4. The constant M presents the approximation accuracy, which is the number of the linear equations [24].

$$\sqrt{\left(PB_{(i,t)}^{Net}\right)^2 + \left(QB_{(i,t)}^{Net}\right)^2} \leq S^{MB} \quad \forall i, t \tag{14}$$

$$\frac{\cos \frac{(2m-1)\pi}{M} PB_{(i,t)}^{Net} + \sin \frac{(2m-1)\pi}{M} QB_{(i,t)}^{Net}}{\cos (\pi/M)} \leq S^{MB} \quad \forall \ i, t \tag{15}$$

$$PB_{(i,t)}^{Net} = P_{(i,t)}^{BD} + P_{(i,t)}^{BC} \quad \forall i, t \tag{16}$$

$$QB_{(i,t)}^{Net} = Q_{(i,t)}^{BC} + Q_{(i,t)}^{BI} \quad \forall i, t \tag{17}$$

The stored energy in the MBESS, $J_{(t)}^{MB}$, should place between the permissible bounds (E_{Min}^{MB} and E_{Max}^{MB}), which is denoted by (18). Besides, stored energy at any time period is a function of the energy stored at the previous time period and the net energy transaction that occurred at the present period. As presented by (19), the net energy transaction is equal to the net charged value minus net injected volume to the bus as discharging energy and energy used for truck movement. The last term is calculated in (7) previously. Finally, as modeled by (20), the energy remaining in the MBESS at the end of time periods has to equal the initial
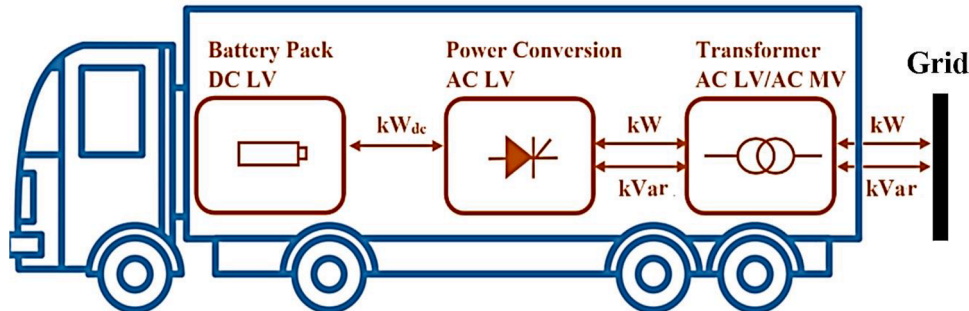
Fig. 2. Various MBESS parts and relevant powers.
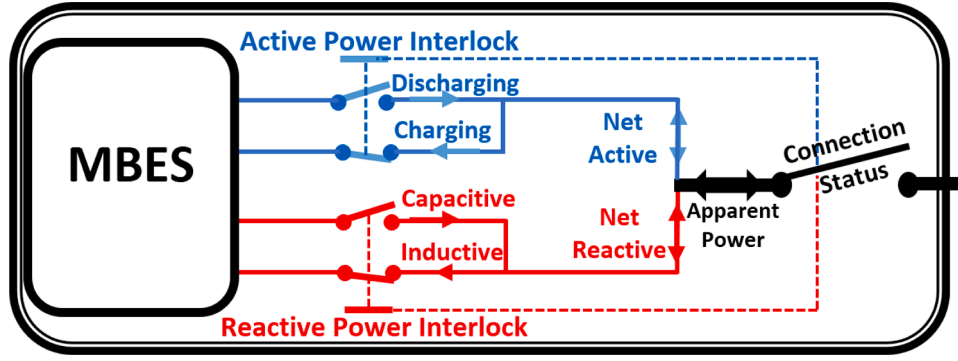
Fig. 3. Relation between active, reactive, and apparent power of the MBESS.
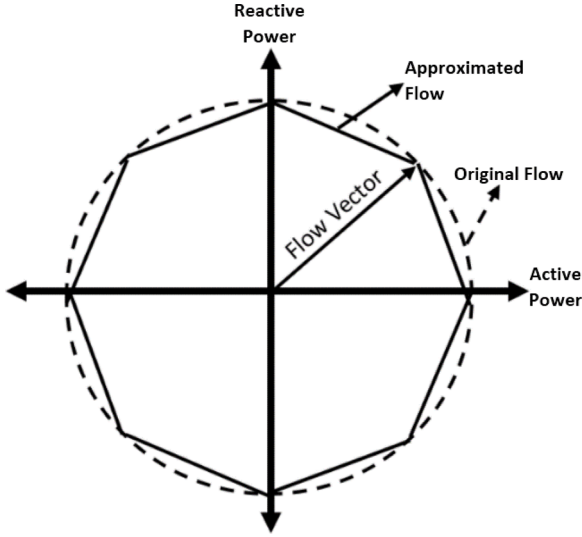
Fig. 4. Apparent power flow limit approximation by a linear polygon.

value (J_{Ini}^{MB}).

$$E_{Min}^{MB} \leq J_{(t)}^{MB} \leq E_{Max}^{MB} \quad \forall t \tag{18}$$

$$J_{(t)}^{MB} = J_{(t-1)}^{MB} + \sum_i P_{(i,t)}^{BC} \eta^{BC} - \sum_i P_{(i,t)}^{BD} \Big/ \eta^{BD} - J_{(t)}^{TR} \quad \forall t \tag{19}$$

$$J_{(t)}^{MB} = J_{Ini}^{MB} \quad \forall t = T \tag{20}$$

3. Integrating mobile battery model in distribution grid optimal power flow

The distribution network operator aims at finding the least cost daily operation schedule. Therefore, the total daily operation cost, *TC*, is defined as the objective function of the problem. This cost is composed of three terms, as formulated in (21). The cost terms forming the objective function are the total daily cost of the energy provided by the up-stream substations (CE_{Tot}^{SS}) and distributed generators (CE_{Tot}^{DG}) in addition to the MBESS' driver cost, explained previously.

$$TC = CE_{Tot}^{SS} + CE_{Tot}^{DG} + CT_{Dr}^{MB} \tag{21}$$

For the substation, the energy cost is a second-order function of the delivered power which can be approximated by a piece-wise linear function [25]. In the piece-wise energy cost, the price of power will be increased by increasing the amount of power. The total cost of the energy provided by the substation is then equal to the summation over all energy price pieces ($\lambda_{(n)}^{SS}$) multiplied by the corresponding generation

block ($\Delta P_{(n,t)}^{SS}$) for all of the time periods, as denoted by (22). The cost of the energy provided by the distributed generators is a linear function of the produced power ($P_{(i,t)}^{DG}$) and price of the power ($\lambda_{(i)}^{DG}$), as declared in (23). The substation's output power at any time period, namely $P_{(t)}^{SS}$, is equal to the summation over all power blocks used for linearization, as denoted (24).

$$CE_{Tot}^{SS} = \sum_{n,t} \lambda_{(n)}^{SS} \, \Delta P_{(n,t)}^{SS} \tag{22}$$

$$CE_{Tot}^{DG} = \sum_{g,t} \lambda_{(i)}^{DG} \, P_{(i,t)}^{DG} \tag{23}$$

$$P_{(t)}^{SS} = \sum_n \Delta P_{(n,t)}^{SS} \quad \forall t \tag{24}$$

The balance of the active and reactive power generation and consumption in the network buses should be kept at any time period. Power generation at any bus of the network includes the distributed generators' contribution and discharged power from the MBES. On the contrary, power consumption is composed of the bus load demand ($P_{(i,t)}^{DM}$), charged power to the MBESS, and summation over line flows ($P_{(i,j,t)}^{LF}$) leaving the bus. It should be noted that the power injection by the substation only exists in bus number 1 of the network. Therefore, network buses' active power balance can be expressed as (25) and (26) for non-substation and substation buses, respectively. Similarly, (27) and (28) present reactive power balance for the network's non-substation and substation buses. In this equations, $Q_{(i,t)}^{DM}$ and $Q_{(i,j,t)}^{LF}$ denote bus reactive load and reactive power flow of the line.

$$P_{(i,t)}^{DG} + P_{(i,t)}^{BD} = P_{(i,t)}^{BC} + P_{(i,t)}^{DM} + \sum_j P_{(i,j,t)}^{LF} \quad \forall i,t, \, i \neq 1 \tag{25}$$

$$P_{(t)}^{SS} + P_{(i,t)}^{BD} = P_{(i,t)}^{BC} + P_{(i,t)}^{DM} + \sum_j P_{(i,j,t)}^{LF} \quad \forall i,t, \, i = 1 \tag{26}$$

$$Q_{(i,t)}^{DG} + Q_{(i,t)}^{BD} = Q_{(i,t)}^{BC} + Q_{(i,t)}^{DM} + \sum_j Q_{(i,j,t)}^{LF} \quad \forall i,t, \, i \neq 1 \tag{27}$$

$$Q_{(i,t)}^{SS} + Q_{(i,t)}^{BD} = Q_{(i,t)}^{BC} + Q_{(i,t)}^{DM} + \sum_j Q_{(i,j,t)}^{LF} \quad \forall i,t, \, i = 1 \tag{28}$$

Finally, active and reactive power flowing through network lines is formulated (29) and (30). In this equations, $g_{(i,j)}^L$ and $b_{(i,j)}^L$ denote line conductance and susceptance, while $\delta_{(i,t)}$ and $\nu_{(i,t)}$ present angle and magnetite of the bus voltage. These are linearized version of the original non-linear newton-based power flow equations. More details on the linearization process and accuracy issues can be found in [26,27].

$$P^{LF}_{(i,j,t)} = g^L_{(i,j)}\left[\nu_{(i,t)} - \nu_{(j,t)}\right] - b^L_{(i,j)}\left[\delta_{(i,t)} - \delta_{(j,t)}\right]$$
$$+ g^L_{(i,j)}\left[\left(\frac{\left(\delta_{(i,t)} - \delta_{(j,t)}\right)^2}{2}\right) + \left(\frac{\left(\nu_{(i,t)} - \nu_{(j,t)}\right)^2}{8}\right)\right] \quad \forall i,t \qquad (29)$$

$$Q^{LF}_{(i,j,t)} = -b^L_{(i,j)}\left[\nu_{(i,t)} - \nu_{(j,t)}\right] - g^L_{(i,j)}\left[\delta_{(i,t)} - \delta_{(j,t)}\right]$$
$$- b^L_{(i,j)}\left[\left(\frac{\left(\delta_{(i,t)} - \delta_{(j,t)}\right)^2}{2}\right) + \left(\frac{\left(\nu_{(i,t)} - \nu_{(j,t)}\right)^2}{8}\right)\right] \quad \forall i,t \qquad (30)$$

4. Case Study

The model introduced in the previous section is tested on a sample system. Accordingly, the model is implemented on the 33-bus distribution test network [28]. The grid single line diagram enhanced with renewable distributed resources and an MBESS is shown in Fig. 5. As can be observed from the figure, the network is powered by the up-stream substation. The solar PV plant and the wind farm are connected to bus 6and bus 33, respectively. To be accounted for real-world situations in terms of parking space and connection limitations, it is assumed that only buses 1, 3, 6, 12, 20, 24, and 31 possess the required conditions for MBESS connection to the network. The selling price of energy by the upstream substation is stair-wise and based on [29]. The hourly load profile for active and reactive power and the produced power by renewable resources is shown in Fig. 6. It is assumed that the network operator owns the renewable distributed generators, and they are not paid for production. The parameters related to the MBESS are as follows.

The power rating and energy capacity are equal to 750 kW and 2000 kWh, respectively, and the charging and discharging efficiencies are the same and equal to 0.96. As a result, the complete round-trip efficiency will be equal to 0.9, which is a conventional figure for the commercial battery system. The initial bus location of the battery is bus 1, and its initial energy is zero. The base case simulation assumes that the total transportation time between all buses is one hour, and the fixed daily driver cost is 50$. Besides, the truck conveying the battery container consumes 2 kWh for hourly movement. The formulation is implemented in the GAMS environment and solved by the CPLEX solver [30].

Simulation results for the critical variables of the problem are shown in Table 1. The table shows the total operation cost, total energy losses, voltage profile index, maximum substation flow, and total cost difference in percent and dollars for the cases without battery and mobile battery. The first case is titled with NBESS indicating no battery energy storage system in the system. The value of the MBESS hourly charging and discharging powers is forced to be zero to achieve simulation results of this case, namely $P^{BC}_{(i,t)} = P^{BD}_{(i,t)} = 0$. In this way, we have a conventional distribution network without a battery energy storage system. The second simulated case, MBESS, denotes the network equipped with the mobile battery energy storage based on the proposed model. In the table, the net total cost difference is obtained by subtracting the total cost in

MBESS case from the NBESS case. Accordingly, the relative cost difference is obtained by dividing the net cost difference by the NBESS case total operation cost. The total energy losses for both cases is calculated by summing up hourly power losses over the time periods, namely 24 hours. The hourly power losses for the whole network can be calculated by adding the loss of each line at any time period. The power loss of each line at any time period, $P^{Loss}_{(i,j)}$, can be calculated by summing up incoming and outgoing powers of the line, as follows.

$$P^{Loss}_{(i,j)} = P^{LF}_{(i,j,t)} + P^{LF}_{(j,i,t)} \qquad (31)$$

The voltage profile index (VPI) is a measure of the flatness of the bus voltages. The ideal value for this index is zero for a case with one per-unit voltage for all of the network buses. AS a result, the lower the VPI value, the smoother the network buses' voltage profile and the lower the voltage fluctuations. Its value can be calculated by summing the network bus voltages for the whole operation period, shown in Eq. (32).

$$VPI = \sum_{(t,i)}\left|1 - V_{(t,i)}\right| \qquad (32)$$

Finally, the maximum substation power flow is the highest value of the apparent power outing from the up-stream substation to supply the network for both cases.

As the results present, the daily operation cost is reduced by 543 $, which means a 4.237 % net reduction. This cost reduction results from price arbitrage and loss reduction achieved by the optimal operation schedule of the MBES. Also, the daily total energy loss is decreased from 4,935 kWh to 4,195 kWh. This reduction, about 15 %, is a direct consequence of the obtained peak shaving by the MBESS deployment. Results of calculating VPI for both cases are equal to 26.358 and 18.314. As these values demonstrate, MBES' optimal schedule helps to flatten the voltage of the network buses. Finally, the substation's maximum flow at the peak load hour is reduced from 4,242 kVA to 3,551 kVA. This reduction can postpone imminent substation expansion plans.

The pattern of the MBESS spatio-temporal status is presented in Table 2. As in the table, the battery remains in the initial bus location, i. e., bus 1, for 5 hours. During these hours, the battery operates in charging mode and is filled up to its energy capacity. Then, it moves to bus 12 during hour 6. The MBESS arrives at bus 12 at hour 7 and stays there until hour 22. During this period, the battery only discharges between hours 16-21, coincides with peak load hours, and is idle at other time periods. Considering that the MBESS must return to its original position at the end of the time interval, it moves from bus 12 to bus 1 during hour 23. The MBESS movement paradigm reveals that it charges at the vicinity of the system's primary power source and discharges at the load centers concerning the bus loads and distributed generators' location.

In order to compare the results, the mobile battery's optimal operation results are compared with a stationary battery. The stationary
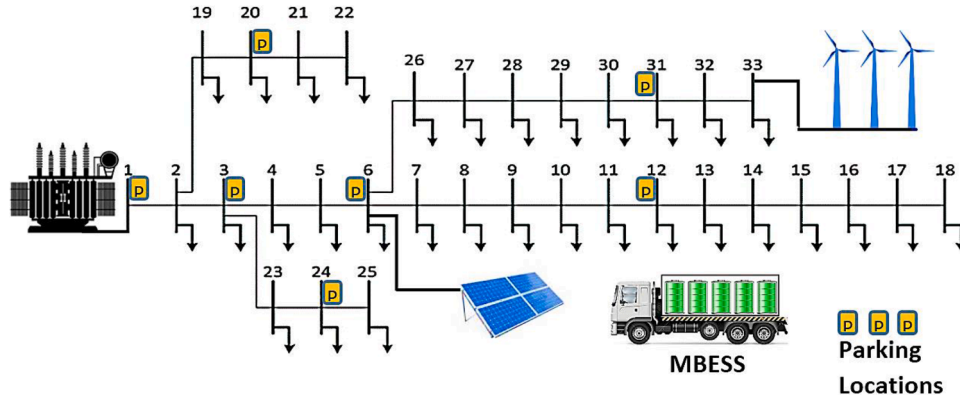
Fig. 5. IEEE 33-bus distribution test case with distributed resources and an MBESS.
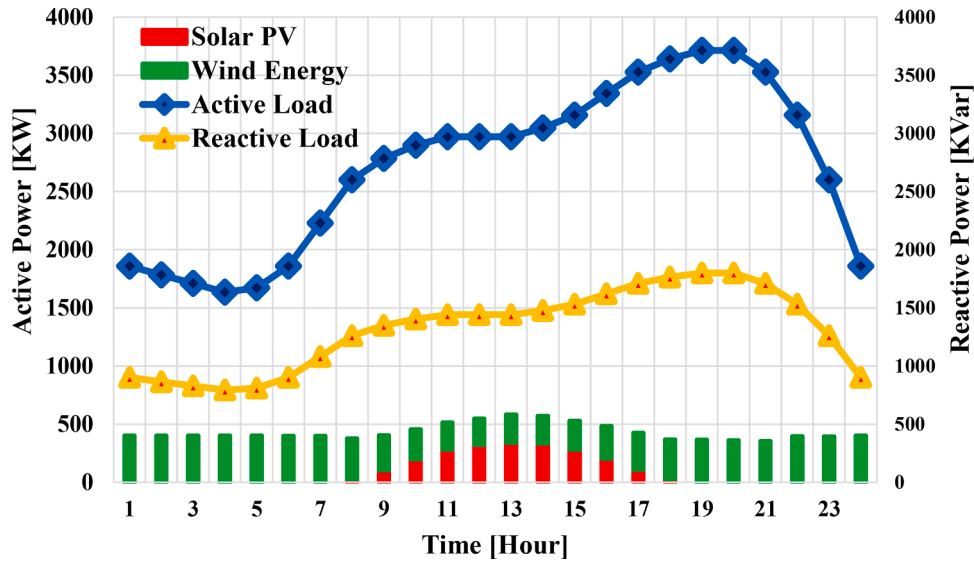
Fig. 6. Hourly active load, reactive load, and renewable distributed generation.

Table 1
Total results of the simulations.

Case Title	BESS Status	Total Operation Cost ($)	Total Cost Difference		Total Energy Loss (kWh)	Voltage Profile Index	Substation Maximum Flow (kVA)
			($)	(%)			
NBESS	None	12,829	-	-	4,935	26.358	4,242
MBESS	Mobile	12,285	543	4.237	4,195	18.314	3,551

Table 2
Transport schedule of the MBESS for the base case simulation.

Hour	Bus	Status
1	1	Charging
2	1	Charging
3	1	Charging
4	1	Charging
5	1	Charging
6	1→12	Transport
7	12	Idle
8	12	Idle
9	12	Idle
10	12	Idle
11	12	Idle
12	12	Idle
13	12	Idle
14	12	Idle
15	12	Idle
16	12	Discharging
17	12	Discharging
18	12	Discharging
19	12	Discharging
20	12	Discharging
21	12	Discharging
22	12	Idle
23	12→1	Transport
24	1	Idle

battery case simulation results can be easily obtained by fixing the spatio-temporal status variables defined in the proposed model. Strictly speaking, for each network bus installed with a stationary battery, it is enough to set the spatio-temporal status binary variable corresponding to that bus to one for all times periods. For example, to have a stationary battery at bus 20 of the system, we have:

$$Z^{MB}_{(i,t)} = 1 \quad \forall i = 20, \quad t \qquad (33)$$

In this way, a stationary battery energy storage can be assigned to

each bus of the system. The results of optimizing the stationary battery's operation for different bus locations are given in Table 3. Besides, the results of the network without battery and one with the MBESS are listed at the top of the table for comparison. As it can be observed, the MBESS results stand top stats with respect to the stationary installation. Strictly speaking, the cost reduction percentage for all stationary bus locations is below the MBESS deployment case. Furthermore, the total energy loss utilizing the MBESS is the minimum with respect to all stationary battery cases. The best results for the MBESS case have not been obtained only for the last two indicators of the table, namely the voltage index and the substation's maximum flow. The reason for this is that the objective target function is focused on the cost of daily operation. It should also be noted that the values obtained for these two indicators utilizing the MBESS are very close to the minimum values obtained for different locations of stationary batteries. The point to note is that the stationary battery can only achieve the desired value of one indicator listed in the table, but employing the MBESS has simultaneously accessed the optimal or near-optimal values of all of them.

The hourly active power charge and discharge schedule and the MBES' stored energy are tabulated in Figs. 7 and 8. As it can be observed, the MBESS works at charging mode during the off-peak period. Then, it delivers charged powers during the peak period, namely hours 16 to 21. In addition, a negligible portion of the stored energy in the MBESS, i.e. 2 kWh, is used for truck movement.

As previously declared, the MBESS can interact with the grid by reactive power inject/withdraw beside active power. In addition to maintaining the bus voltage, this can help reduce line loading by local procurement of the consumers' reactive power. In other words, the reactive current portion of the apparent power flow will decrease. Fig. 9 demonstrates the reactive power exchange of the MBES. As in the figure, the MBESS has only injected reactive power, and its reactive power consumption was zero. This indicates that the network has mainly had a voltage drop problem. In other words, there was no overvoltage problem at any time period to be controlled by the MBESS by means of absorbing

Table 3
Total results for stationary battery with various bus locations.

Case		Cost Reduction Percent	Total Energy Loss	Voltage Profile Index	Substation Maximum Flow
NBESS	-	4935	26.358	4242	
MBESS	4.237	4195	18.314	3551	
Stationary BESS at Bus #	1	2.170	4935	26.358	4242
	2	2.294	4896	26.240	3787
	3	2.982	4662	25.411	3544
	4	3.224	4584	24.694	3554
	5	3.435	4516	23.903	3624
	6	3.988	4335	21.506	3593
	7	4.064	4310	20.279	3590
	8	4.047	4329	19.653	3590
	9	3.982	4370	19.052	3575
	10	3.954	4394	18.274	3569
	11	3.987	4391	18.144	3563
	12	4.016	4391	17.997	3551
	13	3.906	4444	18.504	3548
	14	3.929	4440	18.955	3547
	15	3.910	4451	19.141	3544
	16	3.865	4473	19.488	3538
	17	3.750	4523	19.462	3619
	18	3.625	4574	19.557	3610
	19	2.342	4881	26.349	3899
	20	2.291	4910	26.545	3825
	21	2.276	4919	26.577	3825
	22	2.217	4944	26.585	3827
	23	3.029	4654	25.592	3648
	24	3.025	4672	25.765	3572
	25	2.983	4695	25.876	3581
	26	4.010	4296	21.304	3587
	27	4.105	4237	21.100	3580
	28	4.032	4267	20.417	3573
	29	4.007	4259	20.050	3570
	30	4.102	4248	20.268	3540
	31	4.100	4307	20.194	3566
	32	4.021	4357	20.669	3592
	33	3.905	4398	20.772	3570

reactive power. The voltage profile improvement is a byproduct of load-leveling performed by the MBESS while it is not explicitly modeled. As depicted in Fig. 7, the battery's active power exchange (charging and discharging) at hours 6-15 and 22-24 is zero. Besides, the discharging power of the battery at hours 16-21 is relatively low concerning rated apparent power. As a result, there is an opportunity for the battery to contribute to the voltage regulation at these hours without altering the active power schedule. Accordingly, the MBESS has produced reactive power at hours 7-12 when it is located at bus 12. It should be noted that the battery's reactive power generation or consumption is an inherent capability of its inverter and is denoted by the manufacturers as one of
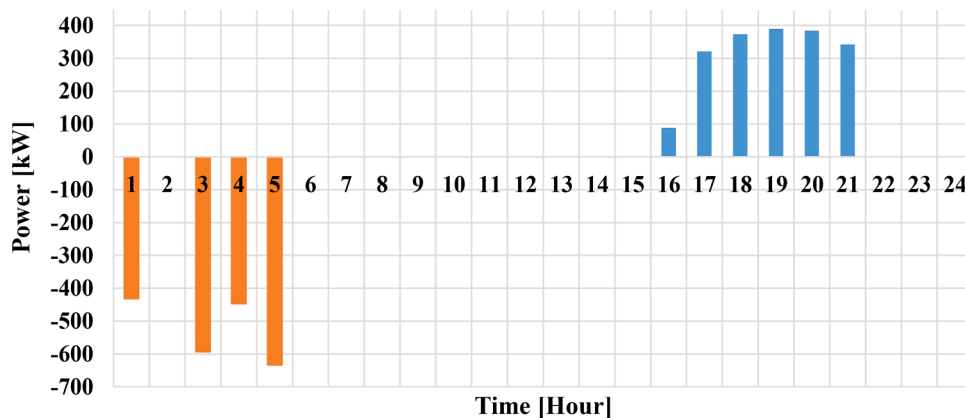
its main strengths. As stated by the manufacturers, this capability has no negative impact on the battery performance, and even it can be in pure inductive or pure capacitive (zero power factor) operation mode.

Active power loss at different hours is presented for the two scenarios in Fig. 10. As can be comprehended from the figure, utilizing the MBESS has reduced losses in most hours of the day. According to the results, the loss reduction is higher during peak hours. The reason for this phenomenon is the ratio of the line losses to the flow of the lines or, in fact, the power passing through them. Since the peak load has decreased during the peak hours, with the optimal scheduling of the MBESS battery, the power losses have also decreased significantly. Another reason for this is the reduction in line flow due to reducing reactive flow share, which has already been described.

Fig. 11 presents the active power drawn from the up-stream substation. As shown in the figure, the peak load is effectively shaved due to utilizing the MBESS. The substation's active power is used to meet the load demand and line losses. Since the MBESS provides a portion of the load demand during peak hours, the line losses will be reduced during these hours. As a result, the active power imported from the substation presents an enhanced decline ratio owing to both reduction resources. Fig. 12 depicts the hourly reactive power drawn from the substation. According to the results, it can be concluded that when the MBESS injected the reactive power, the reactive power produced by the substation was reduced. This means less stress on the substation transformer, less load on the lines, fewer power losses, and energy cost.

Fig. 13 shows the apparent power passing through the grid lines at peak hour, namely hour 20. Accordingly, due to the decrease in both active and reactive power as well as the network losses, the flow of most network lines has decreased. As the figure demonstrates, the reduction in apparent power flow is more significant for lines closer to the substation. Finally, Fig. 14 displays the voltage profile of the network buses
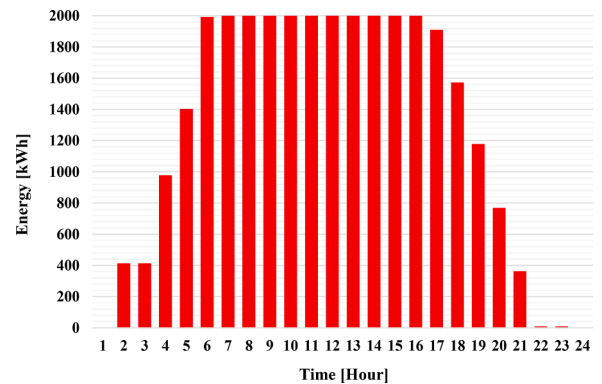
Fig. 8. Hourly stored energy in the MBESS.

Fig. 7. Hourly charge and discharge schedule of the MBESS.
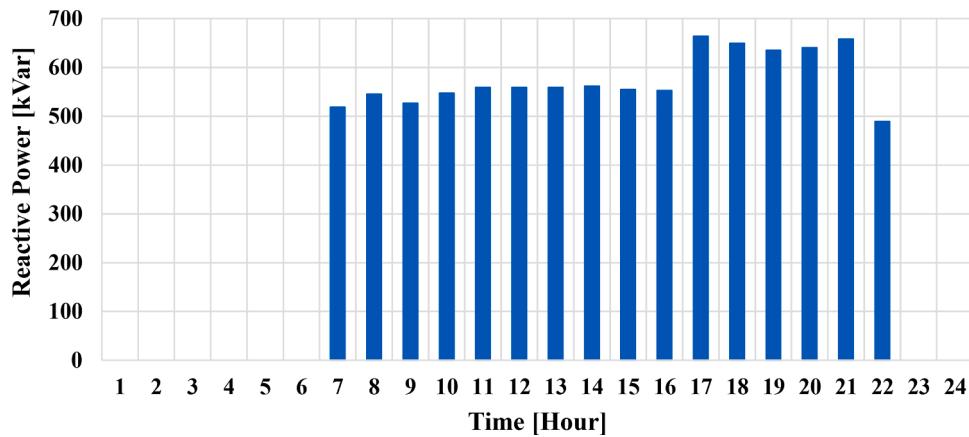
Fig. 9. Output reactive power of the MBES.
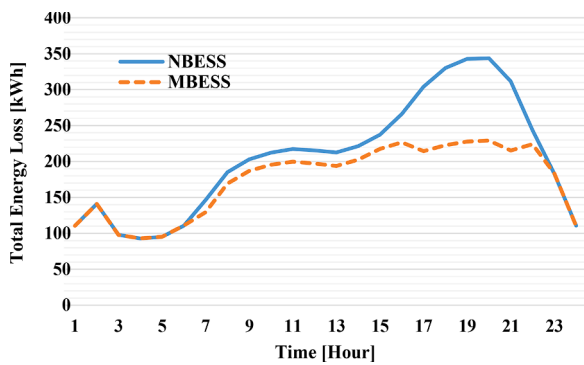
Fig. 10. Network losses for NBESS and MBESS cases.
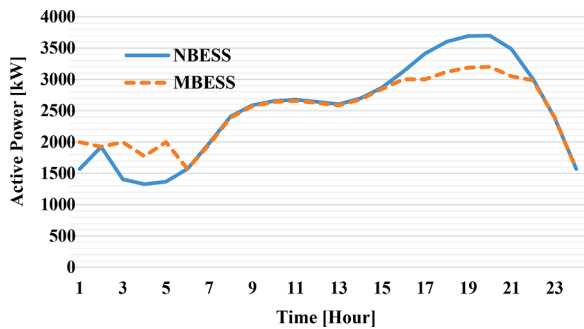
Fig. 11. Active power drawn from the substation for NBESS and MBESS cases.
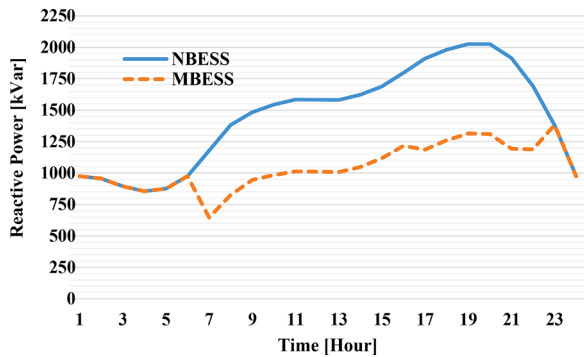
Fig. 12. Reactive power drawn from the substation for NBESS and MBESS cases.

for peak load hour. At this time, the network buses have the highest deviation from the nominal voltage. According to the figure, employing the MBESS has caused a significant decrease in the buses' voltage drop, and their voltage is approaching the nominal value. The reason is the reduction of line loads and the injection of reactive power by the MBES.

A sensitivity analysis is performed concerning changes in critical parameters of the MBESS to evaluate the functionality of the proposed model and analyze its response in different conditions. These parameters include the initial location and total transportation time of the MBES. Accordingly, the initial location of the MBESS is changed between the candidate buses, namely 1, 3, 6, 12, 20, 24, and 31. The results comprising the total cost of daily operation, the difference with the base case without battery scenario, and the percentage of cost reduction plus the number of transports and connected buses are shown in Table 4. As can be seen, the battery's initial bus location has a slight impact on the total cost. In this context, initial bus location 12 offers the highest cost reduction, with 4.289 %. After that, bus 31 is the best initial location in terms of cost reduction. In this case, the MBESS destination bus changes from 12 to 31. Besides, when the MBESS starts the operation period from bus 3, it prefers to charge there and not move to bus 1.

The sensitivity of the results with respect to the transportation time is also evaluated. For simplicity and without loss of generality, it is assumed that all transport between buses has the same required time. In this regard, Table 5 represents the results of changing the transportation time between buses. The transportation time is increased from 1 to 5 hours. Based on the results, cost reduction is highly sensitive to transportation time. This is because as the transport time increases, the MBESS will have less opportunity to connect to the network. Accordingly, the charging and discharging have occurred over a short period of time, and the MBESS will miss the opportunity to inject the reactive power for a long time. In longer transportation times, the time required to charge and discharge the active power will also be very limited. As the results demonstrate for 5 hours' transport time, the cost reduction percentage has reduced significantly.

The proposed model is simulated for 12 daily load profiles to assess its functionality. The daily load factors for these days are calculated utilizing the K-Means clustering method from a whole year (365 days) load factor database provided in [31]. These 12 days are representative days of the whole year. The normalized hourly values for each profile are shown in Fig. 15 separately. As the figure denotes, each profile has a different pattern. Table 6 presents the effect of various daily load profiles in the figure on the main simulation results.

The table contains the total cost difference percentage, MBESS connection buses, voltage profile index, and total daily energy loss. The table indicates that changing the daily load profile will change the main simulation results and even the optimal busses for the MBESS connection. As the results denoted, the total cost reduction percentage varies
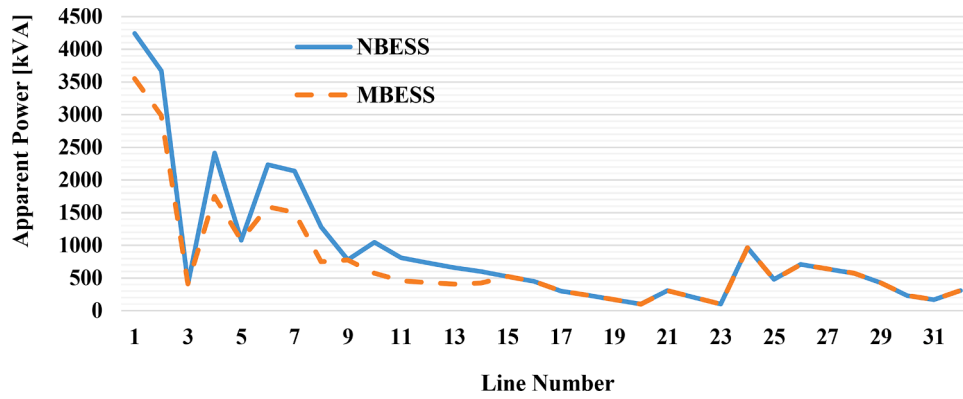
Fig. 13. Line apparent power flows for the NBESS and MBESS cases.
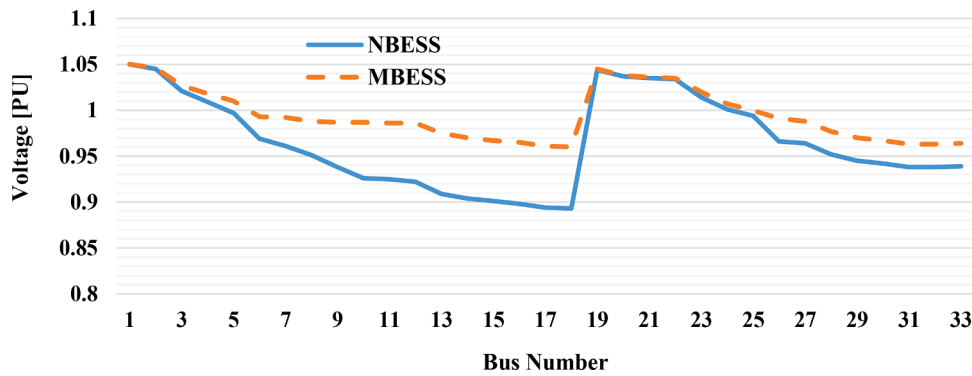
Fig. 14. Bus voltage profile at peak hour for NBESS and MBESS cases.

Table 4
Total cost results for MBESS case with various initial locations.

Initial Location	Total Cost	Difference	
		$	%
Bus 1	12,285	543	4.237
Bus 3	12,292	536	4.182
Bus 6	12,293	536	4.180
Bus 12	12,279	550	4.289
Bus 20	12,296	533	4.156
Bus 24	12,295	533	4.162
Bus 31	12,280	549	4.283

Table 5
Total cost results for MBESS case with various transport times.

Transport Time		1	2	3	4	5
Total Cost	12,285	12,297	12,324	12,387	12,453	
Difference	$	543	532	505	442	375
	%	4.237	4.149	3.938	3.447	2.927

Fig. 15. different daily load profiles used for simulation.

MBESS. Accordingly, the MBESS power rating is changed from 250 kW to 1250 kW with a constant 2000 kWh of energy capacity. Besides, with a 750 kW of fixed power rating, the MBESS energy capacity is changed from 1000 kWh to 3000 kWh. The highlighted rows of the table denote base case values, namely 750 kW and 2000 kWh of, in turn, power rating and energy capacity. As the results indicate, decreasing the MBESS power rating from the base value will significantly decrease the MBESS deployment benefits. Especially, the daily operation cost reduction percentage is reduced with a steeper slope. Based on the results, enhancing the MBESS power rating more than the base value, namely 750 kW, will not improve obtained results. On the other hand, both increasing and decreasing the energy capacity of the MBESS will cause significant changes in the results. As shown in the table, the daily operation cost reduction percentage has been most affected by these changes, which is changed from 2.979 to 5.181.

from 2.023 to 4.159 depending on the load profile. Another point is that, unlike network losses, the maximum reduction in daily operating cost does not necessarily mean the most significant improvement in bus voltages. In other words, a load profile with a significant reduction in daily operating cost may have little impact on improving bus voltage. On the other hand, in line with reducing the daily operation cost, network losses have also decreased. This is because part of the reduction in daily operation cost is related to the reduction of losses in the network due to the flattening of the load profile utilizing the MBESS.

Table 7 represents the sensitivity of the main simulation results concerning changes in the power rating and energy capacity of the

Table 6

Effect of various daily load profiles on the results.

Load Profile	Total Cost Difference (%)	Connected Buses	Voltage Profile Index Difference	Energy Loss Difference (kWh)
P1	3.342	1-12	3.160	518
P2	3.489	1-12-31	3.036	536
P3	3.664	1-12-31	6.105	582
P4	3.789	1-6-12	5.093	531
P5	4.135	1-31	4.793	590
P6	2.023	1-12	2.205	314
P7	3.910	1-6-12	7.105	682
P8	3.880	1-31	0.846	478
P9	3.102	1-12	2.136	403
P10	2.944	1-6-12	0.581	424
P11	2.760	1-12-31	0.188	491
P12	4.159	1-12	6.615	564

Table 7

Sensitivity analysis of MEBSS power rating and energy capacity.

Power Rating (kW)	Energy Capacity (kWh)	Total Cost Difference	Voltage Profile Index	Total Energy Loss (kWh)
250		2.883	22.645	4,437
500		4.091	21.312	4,229
750	2000	4.237	18.314	4,195
1000		4.238	18.276	4,194
1250		4.239	19.280	4,164
	1000	2.979	21.091	4,298
	1500	3.609	20.742	4,243
750	2000	4.237	18.314	4,195
	2500	4.827	18.247	4,158
	3000	5.181	17.604	4,085

5. Conclusions

This paper presents a new model for mobile battery energy storage system (MBESS) optimal operation in distribution networks. The proposed model considered the transportation time and cost of a self-powered electric truck-mounted MBESS by an efficient and straightforward formulation. The proposed model is linear and does not have convergence problems despite its ability to consider the battery's reactive power contribution. Implementing the model on a sample system demonstrates its effectiveness in achieving defined objectives. Accordingly, the total daily operation cost demonstrates a net 543 $ reduction. In addition, the total daily lost energy is reduced by 15 % concerning the case without MBES. Besides, the peak power output of the substation was reduced by more than 16 %. This reduction in the peak load demand has improved the voltage profile across the network buses. In future works, the impact of dynamic changes of the transportation network traffic and off-grid MBESS charging and discharging can be considered.

Funding

CRediT authorship contribution statement

Hedayat Saboori: Conceptualization, Methodology, Software, Formal analysis, Resources, Data curation, Writing – original draft, Visualization, Funding acquisition. **Shahram Jadid:** Conceptualization, Methodology, Validation, Investigation, Writing – review & editing, Supervision, Project administration.

Declaration of Competing Interest

The authors hereby confirm that there's no conflict of interest and financial/personal interest or belief that could affect the objectivity of the work.

References

[1] Y. Su, Smart energy for smart built environment: a review for combined objectives of affordable sustainable green, Sustain. Cities Soc. 53 (2019), 101954.

[2] N. Shaukat, et al., A survey on consumers empowerment, communication technologies, and renewable generation penetration within smart grid, Renew. Sustain. Energy Rev. 81 (2018) 1453–1475.

[3] L. Tronchin, M. Manfren, B. Nastasi, Energy efficiency, demand side management and energy storage technologies–a critical analysis of possible paths of integration in the built environment, Renew. Sustain. Energy Rev. 95 (2018) 341–353.

[4] C. Mejia, Y. Kajikawa, Emerging topics in energy storage based on a large-scale analysis of academic articles and patents, Appl. Energy 263 (2020), 114625.

[5] H. Mehrjerdi, et al., Unified energy management and load control in building equipped with wind-solar-battery incorporating electric and hydrogen vehicles under both connected to the grid and islanding modes, Energy 168 (2019) 919–930.

[6] H. Mehrjerdi, Simultaneous load leveling and voltage profile improvement in distribution networks by optimal battery storage planning, Energy 181 (2019) 916–926.

[7] R. Hemmati, H. Saboori, Emergence of hybrid energy storage systems in renewable energy and transport applications–a review, Renew. Sustain. Energy Rev. 65 (2016) 11–23.

[8] H. Saboori, et al., Energy storage planning in electric power distribution networks–a state-of-the-art review, Renew. Sustain. Energy Rev. 79 (2017) 1108–1121.

[9] MT. Lawder, et al., Battery energy storage system (BESS) and battery management system (BMS) for grid-scale applications, Proc. IEEE 102 (6) (2014) 1014–1030.

[10] H. Hesse, et al., Lithium-ion battery storage for the grid—a review of stationary battery storage system design tailored for applications in modern power grids, Energies 10 (12) (2017) 2107.

[11] Transportable Energy Storage Systems Project, EPRI, Palo Alto, CA, 2009, 1017818.

[12] H.H. Abdeltawab, Y.-R. Mohamed, Mobile energy storage scheduling and operation in active distribution systems, IEEE Trans. Indust. Electron. 64 (9) (2017) 6828–6840.

[13] J. Yan, F. Lai, Y. Liu, C.Y. David, W. Yi, J. Yan, Multi-stage transport and logistic optimization for the mobilized and distributed battery, Energy Convers. Manage. 196 (2019) 261–276.

[14] J. Kim, Y. Dvorkin, Enhancing distribution system resilience with mobile energy storage and microgrids, IEEE Trans. Smart Grid 10 (5) (2018) 4996–5006.

[15] L. Che, M. Shahidehpour, Adaptive formation of microgrids with mobile emergency resources for critical service restoration in extreme conditions, IEEE Trans. Power Syst. 34 (1) (2018) 742–753.

[16] H. Abdeltawab, Y. Abdel-Rady, I. Mohamed, Mobile energy storage sizing and allocation for multi-services in power distribution systems, IEEE Access 7 (2019) 176613–176623.

[17] Y. Song, et al., Multi-objective configuration optimization for isolated microgrid with shiftable loads and mobile energy storage, IEEE Access 7 (2019) 95248–95263.

[18] Y. Chen, et al., Reliability evaluation of distribution systems with mobile energy storage systems, IET Renew. Power Gen. 10 (10) (2016) 1562–1569.

[19] P.M. de Quevedo, et al., Reliability assessment of microgrids with local and mobile generation, time-dependent profiles, and intraday reconfiguration, IEEE Trans. Ind. Appl. 54 (1) (2017) 61–72.

[20] H. Saboori, S. Jadid, M. Savaghebi, Optimal management of mobile battery energy storage as a self-driving, self-powered and movable charging station to promote electric vehicle adoption, Energies 14 (3) (2021) 736.

[21] H. Saboori, S. Jadid, Optimal scheduling of mobile utility-scale battery energy storage systems in electric power distribution networks, J. Energy Storage 31 (2020), 101615.

[22] A. Naderipour, et al., Sustainable and reliable hybrid AC/DC microgrid planning considering technology choice of equipment, Sustain. Energy Grids Netw. 23 (2020), 100386.

[23] S. Dehghan, N. Amjady, Robust transmission and energy storage expansion planning in wind farm-integrated power systems considering transmission switching, IEEE Trans. Sustain. Energy 7 (2) (2015) 765–774.

[24] H. Mehrjerdi, Simultaneous load leveling and voltage profile improvement in distribution networks by optimal battery storage planning, Energy 181 (2019) 916–926.

[25] H. Karimi, S. Jadid, H. Saboori, Multi-objective bi-level optimisation to design real-time pricing for demand response programs in retail markets, IET Gen. Transm. Distrib. 13 (8) (2019) 1287–1296.

[26] Z. Yang, H. Zhong, A. Bose, T. Zheng, Q. Xia, C. Kang, A linearized OPF model with reactive power and voltage magnitude: a pathway to improve the MW-only DC OPF, IEEE Trans. Power Syst. 33 (2018) 1734–1745.

[27] Z. Yang, et al., Solving OPF using linear approximations: fundamental analysis and numerical demonstration, IET Gen. Transm. Distrib. 11 (17) (2017) 4115–4125.

[28] N. Amjady, et al., Adaptive robust expansion planning for a distribution network with DERs, IEEE Trans. Power Syst. 33 (2) (2017) 1698–1715.

[29] Y. Zhang, et al., Optimal placement of battery energy storage in distribution networks considering conservation voltage reduction and stochastic load composition, IET Gen. Transm. Distrib. 11 (15) (2017) 3862–3870.

[30] A. Brook, D. Kendrick, A. Meeraus, GAMS, a user's guide, ACM Signum Newslett. 23 (3-4) (1988) 10–11.

[31] R. Billinton, Power System Reliability Evaluation, Taylor & Francis, 1970.